Assessing food by-products macrocomposition by FTIR microspectroscopy

Paula Varas Perez[1], Alexis Fagot[1], Martijn Heleven[2], Karen Smeets[2], Pieter Samyn[3], Peter Adriaensens[1], Wouter Marchal[1], Dries Vandamme[1*]

[1*]Analytical and Circular Chemistry (ACC), Institute for Materials Research (IMO-IMOMEC), Hasselt University, Agoralaan, Diepenbeek, 3590, Belgium.
[2]Centre for Environmental Sciences (CMK), Hasselt University, Agoralaan, Diepenbeek, 3590, Belgium.
[3]Department of Circular Economy and Renewable Materials, Sirris, Gaston Geenslaan 8, Leuven, 3001, Belgium.

*Corresponding author(s). E-mail(s): dries.vandamme@uhasselt.be;
Contributing authors: paula.varasperez@uhasselt.be; alexis.fagot@uhasselt.be; martijn.heleven@uhasselt.be; karen.smeets@uhasselt.be; pieter.samyn@sirris.be; peter.adriaensens@uhasselt.be; wouter.marchal@uhasselt.be;

Abstract

Food by-products offer a promising opportunity for extracting valuable compounds that can be used in the food, pharmaceutical, and polymer industries. However, unpredictable variations in the chemical composition and spatial distribution of the various components within these biological matrices create challenges for new valorization processes. These inconsistencies can lead to variable recovery efficiency and differing quality of extracts. Understanding the chemical composition and spatial distribution of these components is essential, as it will facilitate the effective valorization of these by-products in future applications.

Fourier transform infrared (FTIR) microspectroscopy was employed to evaluate the chemical composition and structural organization of industrial food by-products, specifically potato trimmings, carrot pomace, and brewer's spent

grain. Frozen sectioning was employed as sample preparation method. Hierarchical cluster analysis was applied to differentiate the spectral information from the background, allowing the determination of representative average spectra with good reproducibility across sample replicates. Derivative FTIR spectra further revealed previously hidden information by resolving overlapping signals, such as multiple bands in the 1750-1550 cm^{-1} region, facilitating the assignment of functional groups to compounds of interest such as proteins, lipids, or pectin and the creation of chemical images. However, some macroconstituents exhibited overlapping absorbance peaks, complicating the precise identification of individual components. Despite this limitation, FTIR microspectroscopy provided valuable semi-quantitative information on the composition of these by-products. The results demonstrated that chemical imaging by FTIR microspectroscopy is a valuable tool for food by-product evaluation, providing insight into their composition and supporting the potential for their valorization in industrial applications.

Keywords: FTIR microspectroscopy, food by-products, composition analysis, cryosectioning

1 Introduction

Annually, more than 10 million tons of fresh mass of food waste are generated in the EU during food processing and manufacture [1]. While reducing food waste is a priority for industries and policymakers, it is acknowledged that some waste generation is unavoidable [2]. Therefore, recognizing unavoidable agricultural and food waste not merely as waste but as a valuable by-product -a feedstock that could be repurposed in other processes- can facilitate the transition towards a circular economy, offering environmental, economic and social advantages [3].

Fruit and vegetable waste is not only generated in large quantities as peels, seeds, pomace, or husks but also holds the potential to be a relevant source of complex compounds such as lipids, proteins, polysaccharides, lignins, or antioxidants [3]. A variety of industrial applications for both macro and microconstituents of food waste have been explored in the literature. These include the extraction of lipids for biofuel production [4], the use of cellulose to develop biopolymers with biodegradable and biocompatible properties [5], and the application of pectin as a gelling and emulsifying

agent [6]. Furthermore, the recovery of plant proteins is essential for the production of meat substitutes tailored to plant-based diets [7]. By-products produced in high volumes worldwide, such as potato trimmings, carrot pomace, or brewer's spent grain, present excellent opportunities for valorization, serving as feedstock in the development of innovative products and applications that offer significant added value.

Potato trimmings (PT) are by-products of the potato industry, consisting of defective fragments trimmed from raw potatoes [8]. Approximately 8 kg of trimmings are generated for every 100 kg of potatoes [9]. Considering global potato production, it is estimated that approximately 30 million tons of potato trimmings are produced annually [10]. The composition of potatoes varies significantly based on their type and the conditions in which they are grown. Excluding water content (78-88%), potatoes primarily consist of starch (9-19%), followed by protein (1.4-2.3%), lipids (0.25-1%), and fiber (0.3-0.75%) [11].

Carrot pomace (CP) is a by-product of carrot juice production, constituting 30% to 50% of the original weight of the carrot [12]. Given that carrot juice represents 50% of the vegetable juice market [13], estimated at over 18 billion liters [14], and assuming a juice yield of 0.5 kg per 1 kg of carrots [15], the global production of carrot pomace could be approximated at 3.6-7.3 million tons. Carbohydrates (46-59%), fiber (20-33%), protein (7-9%), and lipids (0.7-1.1%) are the main constituents of CP after drying, although its exact composition is influenced by the processing method [16].

Brewer's spent grain (BSG) is a by-product generated during the beer manufacturing process. The production of 100 l of beer generates 20 kg of BSG, accounting for more than 38.2 million tonnes worldwide [4, 7]. BSG is primarily composed of residues from barley and other cereals. In particular, it presents a combination of grain husk, pericarp, seed coat, and other endosperm fragments [17]. BSG's composition is rich in proteins (19-30%), lipids (3-10%), lignin (8-28%), and polysaccharides such as cellulose (17-25%), hemicellulose (20-40%) and starch (1-10%). Compositional variations

may occur due to factors such as barley variety, growing and harvesting conditions, or processing [7].

Despite being generated in substantial amounts throughout the year, these by-products are currently employed in low value applications such as animal feed or are discarded. PT, CP and BSG have a great potential to be utilized as feedstock for valorization processes [18–20]. However, the inherent variability in the chemical composition of food by-products, caused by changes in cultivars, processing operations, biological degradation, or storage conditions, presents a challenge in the implementation of new processing methods as it can influence the extraction yield [2]. Additionally, several studies have emphasized the importance of microstructure and its changes in relation to extraction yield [5, 21, 22]. Verwee et al. (2024) demonstrated that a variety of microscopic visualization techniques can be utilized to investigate protein distribution in PT. However, due to the limited specificity of some of these techniques, it was essential to employ a combination of methods to obtain a comprehensive understanding of the protein distribution [23]. Moreover, Belardi et al. (2023) utilized attenuated total reflection–Fourier transform infrared spectroscopy to evaluate the fractionation process of BSG, successfully confirming the extraction efficiency and the utility of spectroscopic methods for precise monitoring of valorization processes [24]. Understanding the precise location and concentration of the compounds of interest in food by-products at different stages of the valorization process could significantly influence the development of more efficient extraction methodologies. Consequently, there is a critical need to develop fast and accurate analytical methods for evaluating food by-product composition.

Fourier-transform infrared (FTIR) microspectroscopy is a promising technique to overview the sample composition and its distribution in a fast, label-free approach [25]. Previous research has demonstrated the efficacy of FTIR spectroscopy in evaluating the compositional attributes of rice, achieving a high degree of accuracy in

the quantification of protein, carbohydrate, and moisture content [26]. In particular, FTIR microspectroscopy has been employed to reveal the compositional distribution of grain barley [27], to locate polysaccharides in bamboo [28], and to identify starch in potatoes [29]. However, the application of FTIR microspectroscopy, in particular in transmission mode, to food by-products is not well established. The measurement of biological samples in transmission mode is preferred as it minimizes the risk of sample damage. This contrasts with attenuated total reflectance mode, where a piston applies pressure, potentially compromising the integrity of the sample [25]. Nevertheless, in order to carry out measurements in transmission mode, samples with a thickness of less than 14 μm are required [30]. Hence, an adequate methodology for sample preparation is required. Traditional sample preparation for FTIR microspectroscopy relies on the preparation of sections from fixed and/or embedded tissue blocks that are mounted on IR-transparent windows to facilitate their sectioning and long-term preservation [25]. This method is time-consuming, and the application of chemicals can hinder the identification of significant signals. Furthermore, fresh samples have the disadvantage of containing water, making them vulnerable to biological degradation. Frozen sectioning is a potential alternative sample preparation method that must be carefully performed to prevent contamination from support media or damage to the cellular structure [25]. Although this method offers benefits such as decreased sample preparation time and the removal of chemical substances for sample embedment, its application to food by-products is, to the best of our knowledge, not yet established.

While the chemical composition of extracts from food by-products has been comprehensively studied, there has been insufficient research into the precise localization of these compounds within the matrix, particularly in untreated food by-products. This gap may be impeding the establishment of effective and profitable valorization processes. The development of analytical methods requiring minimal sample preparation

and offering simultaneous insights into the chemical composition and spatial distribution of food by-products is essential. Additionally, spectral visualization information is complex, with many overlapping signals, and must be carefully pre-treated to extract meaningful conclusions from the rich information collected. The objective of this study is to explore the applicability of FTIR microspectroscopy in food by-product compositional evaluation in terms of their potential for valorization. Frozen sections were used to determine the overall composition of different agri-food by-products, namely PT, CP, and BSG. The reproducibility of the method was addressed after filtering spectral information that was not related to the samples. Key FTIR signals were identified through comparison with existing literature. The analysis of the main signals observed on the average and the second derivative spectra provided valuable insights into the major constituents of the selected food by-products. Additionally, chemical imaging maps were created to assess the spatial distribution of compounds of greater industrial significance such as lipids, proteins or polysaccharides.

2 Methods

2.1 Materials

The study used three streams of food by-products obtained as waste from the food industry: potato trimmings (PT), carrot pomace (CP), and brewer's spent grain (BSG). PT were provided by VEG-i-TEC (UGent, Belgium), and they were collected in a potato company located in Belgium as described in Vanleenhove et al. (2024) [20]. Frozen CP was provided by the Laboratory of Food Technology (KU Leuven, Belgium) after manufacture as described in De Laet et al. (2024) [21]. BSG was obtained from the laboratory Food & Lipids (KU Leuven, Belgium) after being collected in a brewery located in Belgium. Upon reception, all the samples were stored at $-20°C$ until further use for a maximum of 3 months.

2.2 Sample Preparation

Sample preparation was carried out following the method by Liyanage et al. (2017) with some modifications [31]. Briefly, CP and BSG samples were cut into small fragments and placed in a cryomold (4565, Sakura Finetek, The Netherlands). Cubes of 0.5 cm of potato trimmings were cut and placed in closed centrifuge tubes (VWR, Belgium). In all cases, samples were stored in a closed plastic box at $-20°C$ until analysis. Frozen sections were obtained with a cryomicrotome (CM3050, Leica Biosystems, Germany). Frozen samples were mounted onto the specimen holder with a minimal amount of optimal cutting temperature compound (VWR chemicals), transferred to the cryostat chamber, and kept untouched for 30 min to ensure a homogeneous sample temperature. The chamber temperature and the object temperature were previously set at $-18°C$ and $-16°C$, respectively. 10 μm sections of each sample were transferred to CaF_2 windows (Crystran Ltd., UK) for infrared analysis or microscope slides (VWR, Belgium) for microscopy. New blades (Leica 819 disposable blades, Leica Biosystems, Germany) were used for each new set of experiments. At least two technical replicates of each sample were obtained per treatment. Three experimental replicates were obtained by repeating the whole protocol on three different days. Before performing the FTIR microspectroscopy analysis, sections were kept in the dark in a cold room at $5°C$ for 3 hours and inside a desiccator for 30 minutes.

2.3 Microscopic analysis of the structural organization of food by-products

Consecutive sections of the three food by-products (PT, CP and BSG) were examined by Confocal Laser Scan Microscopy (CLSM, LSM900, Zeiss, Zaventem, Belgium) equipped with high-power diode lasers at 405, 488, 514, and 633 nm and mounted on an inverted laser-scanning microscope (Axio Observer Z1/7, Zeiss, Zaventem, Belgium) to visualize their structural organization. The pinhole size was set to 1.00 AU,

which corresponds to 36 μm. Sections of 10 μm were prepared following the procedure described in Section 2.2 but transferred to ultrafrost slides (VWR, Belgium). The autofluorescence (AF) tissue properties of BSG were used to generate micrographs at 40x with a 488 nm wavelength laser (Ex/Em:493/517) at an intensity of 16-18%, a detector gain of 700V and a frame time of 32.72s. Brightfield (BF) micrographs of the three types of samples were imaged using a 40xW LD C-420 Apochromat objective (NA=1.1), with a white light LED intensity set to 5.9% and an exposure time per image of 864 ms. Two experimental replicates were evaluated for each food by-product, imaging at least two different positions in each section.

2.4 FTIR microspectroscopy

FTIR microscopic analyses were performed employing a Hyperion 3000 FTIR microscope equipped with a focal-plane array detector coupled to an Invenio S FTIR spectrometer (Bruker Optics, Germany) based on the method described in Kohler et al. (2007) [32], with some modifications. Samples were measured in transmission mode with a 15x objective for the collection of images of the sample surface. The acquisition parameters were set at 128 scans with no binning at a spectral resolution of 8 cm^{-1} in the spectral region from 4000 to 800 cm^{-1}. The background spectra were acquired from a sample-free area of the CaF_2 window with the same acquisition parameters. After being limited to the region 4000 to 1000 cm^{-1}, spectra were subjected to atmospheric compensation to account for the effect of atmospheric water and CO_2, employing OPUS software (Bruker Optics, Germany). The obtained files were exported and further treated by QUASAR software [33].

2.5 Data processing

2.5.1 Representative average spectrum

A mask was constructed to filter out the regions of samples characterized by very low intensity spectra. Those mostly correspond to the areas where only the support material is present. The hierarchical cluster analysis method proposed by Banas et al. [34] was implemented in the Python [35] language using Spyder 5 [36]. Instead of using a Figure-of-Merit to ensure the stability of the measurement, a combination of the Dunn index and the Davies-Bouldin index was used in order to find the best number of clusters for each sample. On the one hand, the Dunn index represents the ratio of the smallest distance between 2 clusters to the largest distance between data points inside of a cluster; hence, a larger value means better clustering. On the other hand, the Davies-Bouldin index being the mean ratio of cluster scatter to the between cluster separation, a better clustering gives a lower value. Once found, the clusters corresponding to low spectrum intensity regions were used to build a mask to treat the data further. Baseline correction followed by standard normal variate normalization was applied to all spectra to compensate for undesired variations. The mask was applied to the normalized data to filter out the pixels corresponding to low intensity spectra. The representative average spectra were then computed with the remaining pixels.

2.5.2 Chemical imaging

After reducing the spectral region to the range 1800-1000 cm^{-1}, the average second derivative spectra were calculated, employing a Stavitsky-Golay algorithm (polynomial order 2, window size 9) to smooth spectra and resolve overlapping signals [32]. The assignment of the principal absorption bands was performed based on a literature study. Chemical imaging was carried out using QUASAR software [37]. The image construction was performed by integrating the area of the relevant peaks found on the

second derivative spectrum of each sample. False color maps were generated representing the intensity of the bands throughout the sample surface, providing information about the spatial distribution of functional groups related to compounds of interest.

3 Results and discussion

3.1 Microscopic analysis of the structural organization of food by-products

Given the limited magnification of FTIR microspectroscopy, BF and CLSM were employed as complementary techniques to investigate the microstructure of the food by-products further. This approach enabled higher-resolution imaging of cellular structures, which could not be resolved by FTIR microspectroscopy. Spatial resolution is a critical factor in the performance of a chemical imaging system, as it measures the ability to distinguish between closely spaced objects. In FTIR microspectroscopy, as in all forms of optical microscopy, spatial resolution is constrained by the diffraction limit. This diffraction limit is directly proportional to the wavelength of the incident light and inversely proportional to both the index of refraction and the numerical aperture of the objective lens. The theoretical lowest spatial resolution achievable with an FTIR microscope is 3.81 μm at λ=2.5 μm. However, various instrumental factors may influence the effective resolution, potentially resulting in higher values [38]. The limited resolution of FTIR microspectroscopy might lead to uncertainty in the interpretation of spatial information. Hence, the combined use of BF, CLSM and FTIR microspectroscopy provides a more comprehensive understanding of the microstructural organization of food by-products.

Consecutive sections of frozen samples were prepared for potato trimmings (PT), carrot pomace (CT), and brewer spent grain (BSG). BF micrographs (Fig. 1) were collected to provide additional information on the structural organization of food by-products at the cellular level.

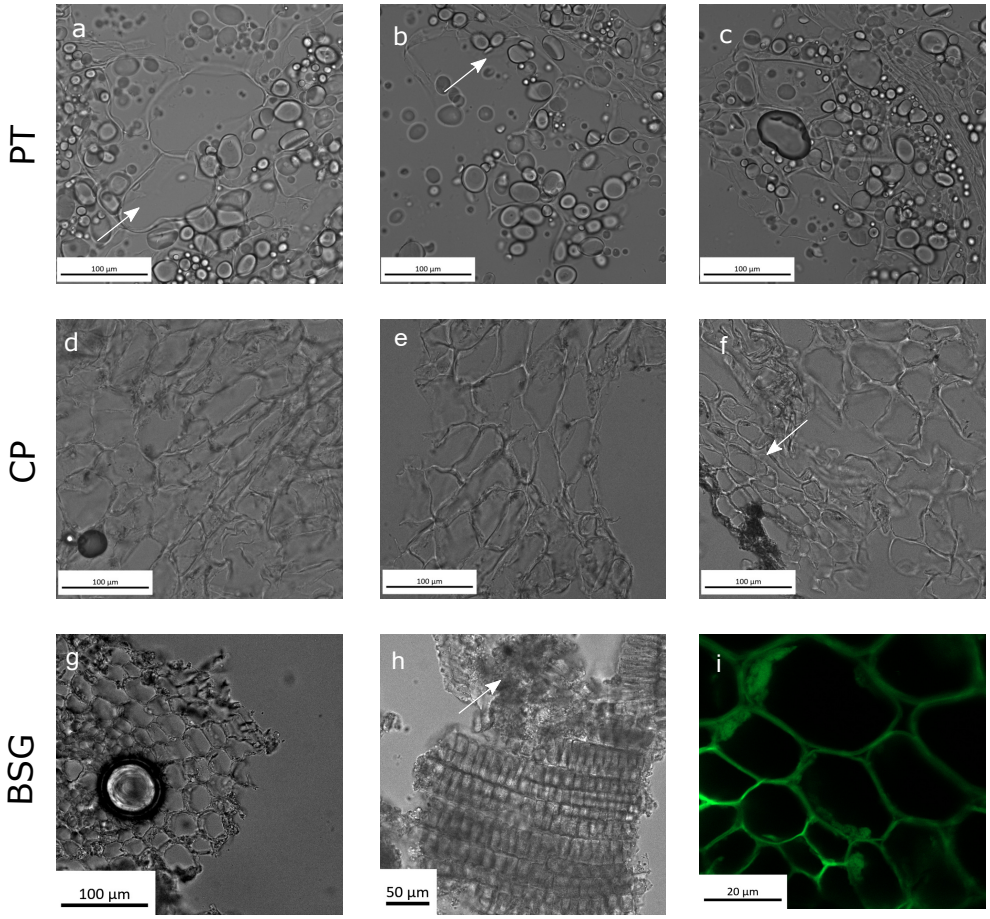

Fig. 1 Visualization of Potato trimmings (PT) (a-c), Carrot pomace (CP) (d-f), and Brewer's spent grain (BSG) unstained sections obtained by brightfield microscopy (BF) (a-h) and confocal laser scan microscopy (CLSM). The sections are 10 μm thick, cut by cryotome. (a-c) Transverse cross-sections of PT. (a) The arrow points to an empty cell. (b) The arrow points to a damaged cell wall. (d-f) Longitudinal cross-section of CP. (f) The arrow points to cell layers separated. (g-h) Longitudinal cross section of BSG. (h) The arrow points to a multilayer of tissue generated after sectioning that hinders microscopic observations. (i) Visualization of the autofluorescence properties of the tissue BSG at 488 nm excitation, reflecting the distribution of lignin and phenolic compounds.

The BF micrographs of PT showed a relatively intact polygonal cell wall structure with starch granules located inside the cells (Fig. 1a-c). A few damaged cell walls

are observable; however, it remains challenging to determine whether the damage was produced during industrial processing or the sectioning process. Some empty cells can be found due to the loss of starch granules on potato cells after sectioning (Fig. 1b), as previously reported by Sjoo et al. [39]. Besides the inherent variations in the size and shape of cells depending on their cultivar and type of cell [40], changes in structure can be attributed to the peeling or freezing process, which can cause starch gelatinization and changes on the cell wall, respectively [20, 41].

Untreated carrot tissue typically shows polygonal parenchyma cells of uniform size and compact, ordered arrangement. BF micrographs of CP displayed fragments of compact cell wall structures, where the integrity of the plant tissue was mainly lost (Fig. 1d-f), in concordance with Sucheta et al. [42] and Amoroso et al. [12]. In addition, some separation among the cell layers can be observed, probably originating from the freezing process (Fig. 1f) [41]. Those microstructural changes could have originated from the application of pressure required for the industrial production of carrot juice [43]. Knockaert et al. demonstrated that blended carrot puree tissue is composed by large cell clusters, with a negligible number of single cells present [44]. This observation is consistent with our findings.

The adhesion of BSG to the CaF_2 crystals was substantially lower compared to PT and CP, which made it more difficult to obtain large, high-quality sections (Online Resource A). Nevertheless, the tissue sections that were successfully transferred to the support crystal maintained their structural integrity, as illustrated by Fig. 1g-h. The distinct variations in cell types observed can be attributed to the diversity of tissue types present, which aligns with the heterogeneous composition of the BSG [45]. Generally, BSG is described as a lignocellulosic material rich in protein and fiber [46], and composed of intact layers of aleurone cells, which primarily store protein and large clusters of connective endosperm proteins [17]. Our results align with these descriptions as seen in Fig. 1g-h. It is important to note that the heterogeneous size of BSG

impedes the alignment of all sample material in the same direction. This can result in multilayers of tissues after sectioning and generate areas of sample material not suitable for microscopic observations (Fig. 1h). The CLSM micrograph shown in Fig. 1i revealed autofluorescence at 488 nm excitation. The presence of lignin and aromatic substances such as polyphenols and flavonoids is known to produce autofluorescence in the aleurone cell walls of barley, [47], demonstrating the integrity of the cell walls in BSG fragments.

It is important to note that PT and CP were also analyzed through CLSM; however, the autofluorescence observed proved to be uninformative. On the one hand, CP contains carotenoids that emit autofluorescence in the 400-600 nm range [48], which generates excessive signals and cannot be employed to assess cellular integrity effectively. On the other hand, PT displayed autofluorescence, although it was not uniformly distributed throughout the sample. PT has a lower lignin content, as its formation during the wound healing process occurs gradually. Regions of higher intensity likely indicate the accumulation of fluorophores such as suberin [49, 50].

3.2 Obtaining a representative average spectrum

After the transference of the sections to the CaF_2 crystals, areas free of sample could be observed. Fig. 2a provides an example of this situation in the case of BSG, but the same phenomena can be observed on PT and CP samples. These areas, where water was located in frozen conditions, consisted exclusively of support material during spectral acquisition. As a result, the spectral information gathered from these regions does not accurately reflect the chemical composition of the sample and could lead to the incorrect calculation of the average IR spectrum representative of each sample. As the tissue is not homogeneously distributed throughout the surface, it is necessary to treat the data to exclude as much spectral information not related to the sample as possible from the analysis. By going through the data pixel by pixel, the difference

between support material and tissue spectra can be distinguished as follows. When measuring tissue, the obtained spectrum displays relatively high absorbance values, contrary to the spectrum measured in a sample region with little to no tissue where the spectrum intensity is small. This property of the spectra is seen in Fig. 2e and can be exploited to group the pixels with similar intensity into clusters using hierarchical cluster analysis.

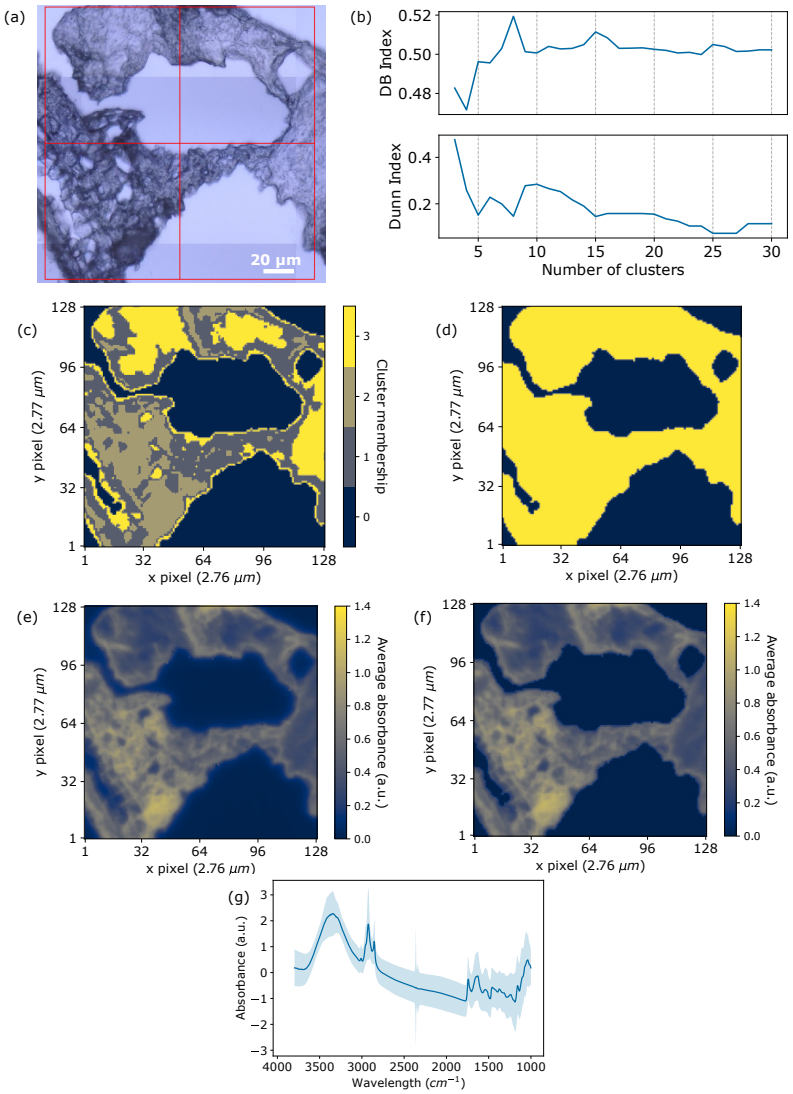

Fig. 2 (a) FTIR micrograph of a BSG sample where the areas free of sample are visible in light gray. (b) Evolution of the Davies-Bouldin (top) and Dunn (bottom) indexes of the sample with increasing number of clusters (Davies-Bouldin index minimum: 4 clusters, Dunn index maximum: 3 clusters). (c) Clustering using 4 clusters (0: black, 1: gray, 2: khaki, 3: yellow). Pixels in cluster 0 correspond to the areas without sample. (d) Corresponding mask used for the filtering (black: areas to filter out, yellow: BSG sample). (e) Average absorbance intensity map before filtering (scale: low intensity in black to high intensity in yellow). (f) Average absorbance heatmap after filtering (scale: low intensity in black to high intensity in yellow). (g) Representative average spectrum with 95% confidence interval, indicated by the colored area, using hierarchical cluster analysis.

This method is based on an algorithm that compares pairs of pixels and groups the pairs that are closer together in terms of mean absorbance. The clustering was specifically performed using Ward's algorithm which aims at minimising the total variance within clusters. In their analysis, Banas et al. [34] made use of both the Dunn index [51] and the Figure-of-Merit [52] to respectively measure the inter connectivity and the stability of the clustering. Nevertheless, the calculation of the latter being computation heavy for samples of 128 x 128 pixels, a combination of the Dunn index and the Davies-Bouldin [53] index was used instead. As both indicators might point to a different best number of clusters, a compromise between a high Dunn index and a low Davies-Bouldin index was sought for each sample to reach the best result. The clusters corresponding to the regions with low intensity spectra were then filtered out. Removal of the spectra not related to the tissue allowed the extraction of a good quality average spectrum that can serve to compare the signals of samples with different origins or treatments.

In the case of the sample presented in Fig. 2, Fig. 2b shows that the best clustering is achieved for 3 clusters with the Dunn index and 4 with the Davies-Bouldin index. After the empirical assessment, 4 clusters were chosen for the sample, as can be observed in Fig. 2c. Indeed, with 3 clusters, large parts of what is seen here as cluster 3 were grouped together with the area without sample and corresponding to cluster 0. Cluster 0 was then used to constitute the mask shown in Fig. 2d to filter the data in Fig. 2e, as can be seen in Fig. 2f. As a result, the representative average spectrum presented in Fig. 2g was obtained using all the pixels that were not filtered. The signals obtained followed the trends expected for biological materials. The same method was applied to all samples, providing similar results (Online Resource C-D). Representative average spectra of each sample, including a detailed description of the peak assignment, can be found in Online Resource F.

3.3 FTIR microspectroscopy analysis

In the first place, the reproducibility of the sample preparation was confirmed by collecting the average spectra of three consecutive sections of the same sample prepared on the same day, as well as sections from the same material prepared on different days. For each section, an average spectrum was obtained following the method described in Section 3.2. The spectral position of the peaks remained consistent across the different sections of the same sample, although intensity variations can be observed in BSG due to the low adhesion of the sections to the crystals. Furthermore, the position of the signals is comparable for samples measured on different days (Online resource E). Therefore, any shift in the position of the signals can be attributed to changes in the food by-products rather than variability induced by the sample preparation method.

Major constituents of biological samples are proteins, lipids, and polysaccharides, with varying ratios depending on the type of plant material. The chemical specificity of FTIR microspectroscopy enables the identification of the major constituents of food by-products by correlating the observed signals with relevant components found in the literature. Due to their chemical characteristics, most of the bands related to their functional groups overlap with other signals, impeding the identification of individual peaks. To obtain more information about the specific composition of the three different food by-products, a more detailed study of the signals was performed using a second derivative. The second derivative spectra of PT, CP, and BSG are shown in Fig. 3a, Fig. 3b, and Fig. 3c, respectively. Using this technique in spectroscopy is advantageous as it enhances the separation of overlapping signals [32]. Although some signals specific to certain components could be identified, most bands still overlapped due to the complex composition of plant materials. Table 1 collects a summary of the relevant signals observed, the compounds associated, and the food by-product where they can be found.

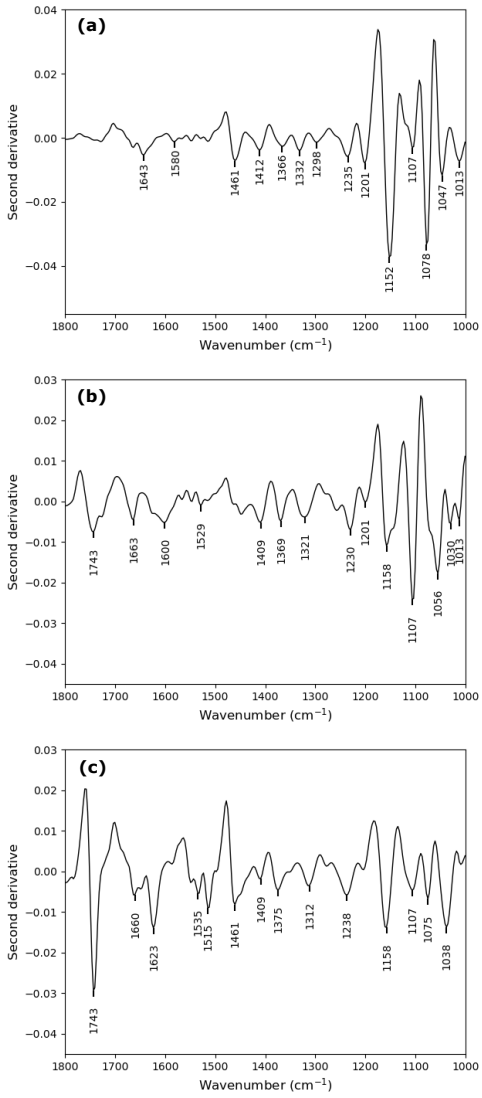

Fig. 3 Second derivative spectrum of (a) potato trimming (PT), (b) carrot pomace (CP) and (c) brewer's spent grain (BSG).

Liang et al. reported the presence of an absorption band at 1746 cm^{-1}, which was attributed to lipids and suberin [54]. However, this peak was not clearly visible in the second derivative spectrum of PT (Fig. 3a) despite lipids and suberin accounting

Table 1 Main absorption bands found in potato trimmings (PT), carrot pomace (CP), and brewer's spent grain (BSG), their vibrational mode assignment, and their corresponding compound.

Wavenumber (cm^{-1})	Vibrational Mode Assignment	Characteristic Compounds	Food By-product	References
1746	C=O stretching	Lignin, suberin	PT	[54]
1743	C=O stretching	Pectin, β-carotene, lipids, lignin, hemicellulose	CP, BSG	[6, 16, 27]
1700-1600	H-O-H bending vibration, COO^- antisymmetric stretching	Water, pectin, amide (protein), phenolic compounds	PT, CP, BSG	[54–57]
1461	Asymmetric deformation of aromatic CH_2 and CH_2 bending	Lignin, starch	PT, BSG	[18, 27, 58]
1369	CH_3 bending vibration, C-H bending	Carotenoids, cellulose, hemicellulose	CP	[57, 59]
1235-1230	Amide III, C-O stretching	Protein, pectin	PT, CP	[55, 56, 60]
1150-1100	C-O, C-C, C-OH stretching	Starch, cell wall polysaccharides	PT	[56, 58]
1100-1000	C-O-H bending, C-O stretching	Starch, cell wall and ring polysaccharides	PT, CP, BSG	[46, 55, 56, 61]

for the 0.1-0.5% and 0.1% of the fresh potato tuber weight, respectively [62, 63]. The absorption band located at 1643 cm^{-1} may be attributed to the amide I [54]. The signal visible at 1235 cm^{-1} has been assigned to proteins (amide III) [56], but it might be overlapping with the C-O stretching associated with pectin, reported at 1260-1230 cm^{-1} [55]. The band found at 1461 cm^{-1} is generally attributed to the asymmetric deformation of C-H groups found in the aromatic part of lignin [18] but could also reflect the CH_2 bending of starch [58]. Starch signals have also been reported to appear at 1150-1100 cm^{-1} (C-O, C-C, C-OH stretching) and at 1100-900 cm^{-1} (C-O-H bending) even though other polysaccharide bands could also be found between 1200-800 cm^{-1}. In particular, the peaks at 1152, 1107, and 1078 cm^{-1} have been described to belong to the stretching bands of cell wall polysaccharides[56, 58].

The second derivative spectrum of CP shows multiple bands in the region 1800-1000 cm^{-1} (Fig. 3b). The peak at 1743 cm^{-1} is generally assigned to the C=O stretching from methyl esterified carboxyl groups that can be found in pectin [6]. A broad band is seen centered at 1600 cm^{-1} that could be attributed to the overlapping of the H-O-H bending vibration of water and the COO- antisymmetric stretching vibrations found in pectin, amides, and phenolic compounds [55, 56]. The existence of a band at 1369 cm^{-1} is related to either the bending vibration of the methylene group present in carotenoids or the C-H bending of cellulose and hemicellulose [57, 59]. The signal at 1230 cm^{-1} is likely to be related to the C-O stretching vibration of galacturonic acid [60], which constitutes the linear skeleton of pectin and can be an indicator of the amount of pectin present in the sample [64]. In addition, the band at 1013 cm^{-1} has been associated with the C-O stretching of pectin [55]. However, this signal could overlap with cellulose or ring polysaccharides [55, 56].

In BSG (Fig. 3c), the intense peak at 1743 cm^{-1} could be attributed to the stretching vibration of the C=O bond found in lipids, lignin or hemicellulose [18, 27].

Moreover, the broad signal observed at 1461 cm^{-1} is usually associated with the C-H bending of lipids [27]. However, this signal may also have originated due to the presence of lignin, hemicellulose or starch [18, 58]. Furthermore, our results show the characteristic aromatic skeletal bands characteristic of lignin around 1515 cm^{-1} [46]. In addition, the intense peak at 1623 cm^{-1} could correspond to the aromatic hydrocarbons of lignin [57]. The signal at 1660 cm^{-1} could be assigned to the amide I in barley, but it is not too prominent in our results [27]. Additionally, the peaks located at 1535 and 1238 cm^{-1} can be associated with amide II and amide III bands, although signals related to lignin or hemicellulose can also be found in the first and the second [24, 46]. Finally, multiple bands are found between 1160-1000 cm^{-1} and can be related to the C-O, C-OH, or C-C stretching modes of polysaccharides such as starch, cellulose, hemicellulose, or lignin [46, 61].

The major advantage of FTIR microspectroscopy is the simultaneous acquisition of spectral and spatial information over large areas in a short time. Absorption profiles are recorded through the sample, and false color chemical maps can be created based on the intensity of those signals [25]. False color maps show the distribution of target compounds through the sample, providing tools to investigate changes in the composition and distribution of industrially relevant macroconstituents.

Visualization of the distribution of the main constituents of PT, CP, and BSG in cryosections was performed by integrating the main signals obtained in the derivative FTIR spectrum. This procedure enables the creation of false color maps as the area of a second derivative peak is proportional to the area of the corresponding peak in the original spectrum [65]. Fig. 4a-d, Fig. 5a-d and Fig. 6a-d collect the micrograph and the false color images obtained after the integration of the relevant signals of PT, CP, and BSG, respectively. The false color scale ranges from low absorbance (red) to high absorbance (blue).

FTIR microspectroscopy was applied to assess the lipid, lignin, starch, and protein distribution across the PT section. The PT micrograpgh (Fig. 4a) shows a high amount of globular structures. Despite the low intensity of the band at 1746 cm^{-1}, the distribution map shows a moderate concentration of suberin and lipids in the sample (Fig. 4b). Lipids are located in the cell membrane and in the form of lipid droplets while suberin is mainly located in the periderm [62, 63]. As the micrograph shows flesh tissue, it is possible to attribute the signal to lipids, proving a higher accumulation of lipids in the areas where the cell wall is located. However, pectin could also contribute to the distribution map as it is also located in the cell walls [6, 39]. The characteristic globular structures found in the distribution map of the band at 1461 cm^{-1} (Fig. 4c) suggest a higher contribution of starch than lignin. The distribution map of the peak centered at 1235 cm^{-1} shows a similar distribution (Fig. 4d) than the peak centered at 1461 cm^{-1} with a higher intensity around the starch globules. Potato protein is located mainly in the vacuoles of the parenchyma tissue in tubers [66], but cell wall disruptions during potato processing could lead to the creation of hydrogen bonds between protein and starch.

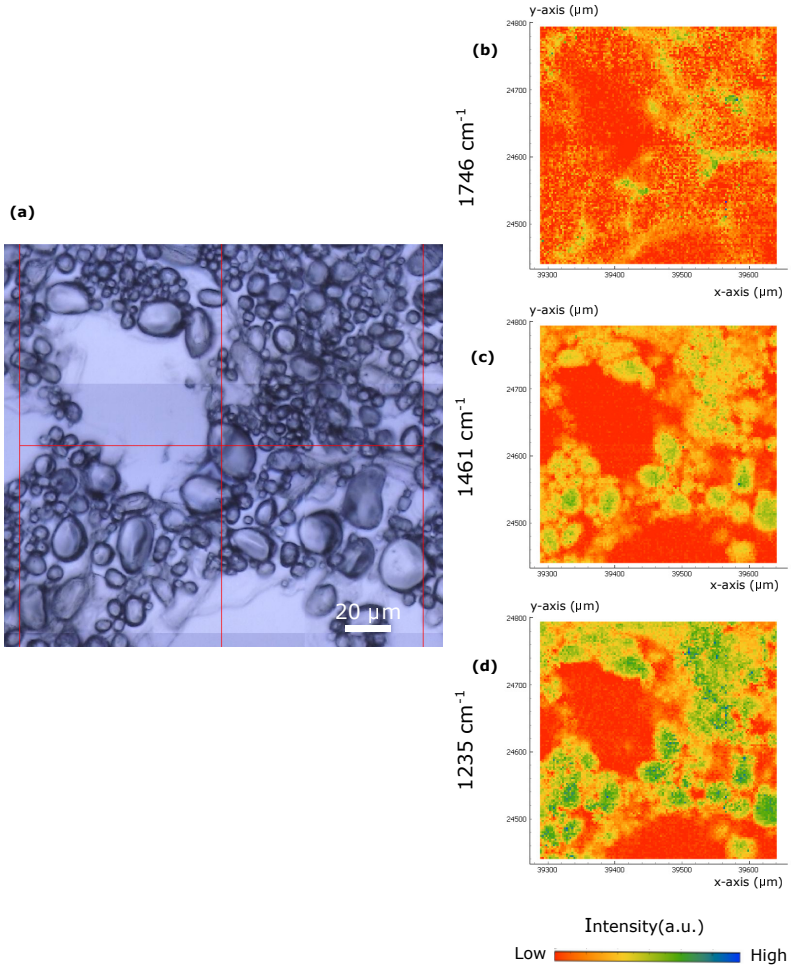

Fig. 4 Distribution of main components of potato trimmings (PT) by FTIR microscopy in transmission mode. (a) Micrograph (b) Lipids and suberin distribution based on the IR absorption at 1746 cm^{-1} (c) Lignin and starch distribution based on the IR absorption at 1461 cm^{-1} (d) Protein and pectin distribution based on the IR absorption at 1235 cm^{-1}. The IR adsorption intensity increases from red to blue. Scale bar = 20 μm

The chemical imaging of CP was focused on cellulose, hemicellulose and pectin. The CP micrograph shows a mixture of disrupted and compact cell wall structures (Fig. 5a). The IR bands at 1746, 1369, and 1158 cm^{-1} were used to visualize the distribution of pectin, carotenoid/hemicellulose/cellulose and pectin/cellulose, respectively.

Pectin is usually found in the middle lamella of the cell wall of carrots and has an important role in its barrier properties [42]. When comparing the distribution maps of the band at 1746 cm^{-1} (Fig. 5b) and the band at 1158 cm^{-1} (Fig. 5d), we observe a similar distribution of the signals, with more dispersed structures in the latter band. Additionally, higher intensity is observed in both cases in regions where the cell structure is more intact, although the intensity is higher in the map corresponding to 1746 cm^{-1}, reflecting the more intense peak as shown in Fig. 3b. At 1369 cm^{-1} (Fig. 5c) a similar distribution is observed, but the borders are less defined, probably due to the additional contribution of hemicellulose and carotenoids. Although the stress caused by juice extractions leads to changes in secondary metabolites, which results in the loss of almost half of the β-carotene during the conversion of fresh carrots to pomace, the presence of cell walls may prevent the release and help the retention of β-carotene [19]. However, the low concentration of carotenoids in carrot pomace compared with the bulk of the material might mask the contribution of carotenoids to the 1369 cm^{-1} signal. Finally, the distribution of the three maps (Fig. 5d) can provide additional information about the cell wall integrity as cellulose, hemicellulose and pectin are three of the major components of plant cell walls [56].

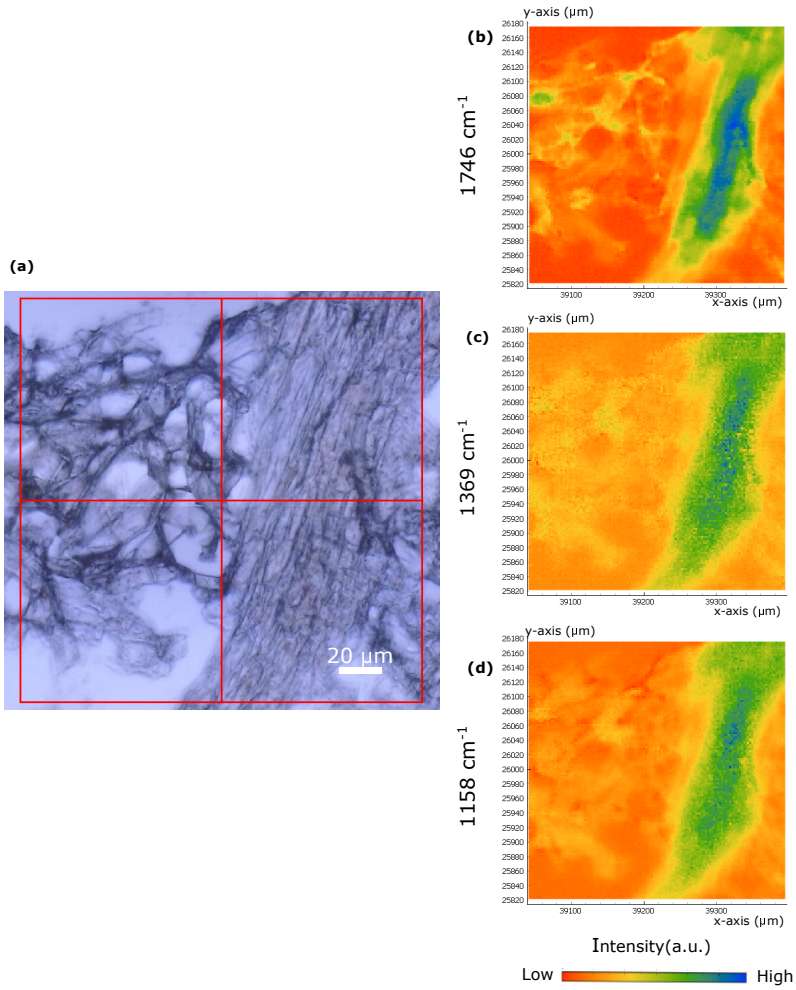

Fig. 5 Distribution of main components of carrot pomace (CP) by FTIR microspectroscopy in transmission mode. (a) Micrograph (b) Pectin distribution based on the IR absorption at 1746 cm^{-1} (c) Hemicellulose, cellulose and carotenoids distribution based on the IR absorption at 1369 cm^{-1} (d) Pectin and cellulose distribution based on the IR absorption at 1158 cm^{-1}. The IR adsorption intensity increases from red to blue. Scale bar = 20 μm

In the present study, the second derivative spectral bands at 1746, 1461, and 1180-1000 cm^{-1} were employed to generate chemical images of lipid/lignin/hemicellulose, lipid/lignin/starch, and polysaccharide distributions in BSG, respectively. Despite the poor adhesion of BSG to the support material, it is possible to discern differences in

the distribution pattern of lipids, lignin, and polysaccharides. The BSG micrograph (Fig. 6a) presents distinct types of tissue. At the bottom left the husk can be found, which continues to a layered and packed cell structure attributed to the pericarp, followed by fragments of the aleurone border, connected with some parts of the solubilized endosperm [27]. Imaging the 1180-1000 cm^{-1} region (Fig. 6d) provides valuable insights into the polysaccharides present in the sample. While lignin may show signals in this region, the bands related to polysaccharides are expected to be more pronounced and predominantly displayed [61]. The high intensity region shown in blue could be related to the presence of starch in the residues of the endosperm, which may be retained after the mashing process [67]. A detailed analysis of the second derivative spectral bands of this region supports this hypothesis (Online Resource G). The false color map corresponding to the 1461 cm^{-1} peak (Fig. 6c) illustrates comparable structures; however, it indicates distinct areas with elevated concentrations. The higher intensity observed in the pericarp can be attributed to the lignified cell walls of the maternal layers [47]. In contrast, the intense regions found in the aleurone layer result from the presence of polysaccharides, phenolics, and lipids, as the aleurone does not contain lignin; instead, hemicellulose primarily contributes to the signal as demonstrated in the Online Resource H. A comparison with the previous false color maps shows that the areas exhibiting higher concentrations in the 1746 cm^{-1} imaging (Fig. 6b) can be attributed to lipids and lignin derivatives [57].

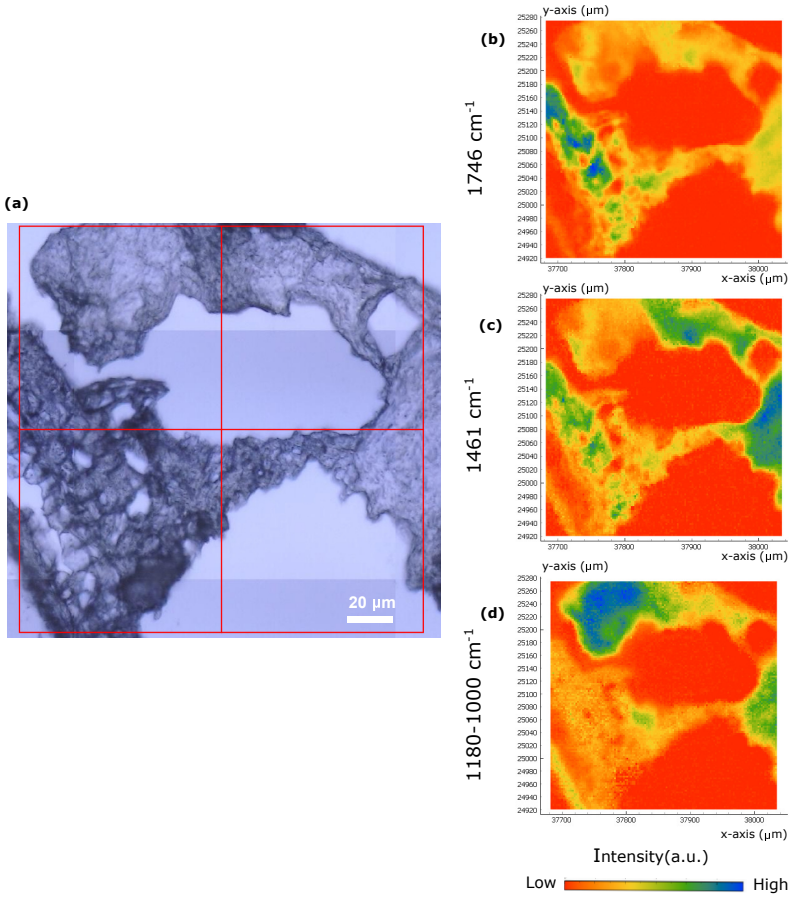

Fig. 6 Distribution of main components of brewer's spent grain (BSG) by FTIR microspectroscopy in transmission mode. (a) Micrograph (b) Lipids, lignin, and hemicellulose distribution based on the IR absorption at 1746 cm^{-1} (c) Protein distribution based on the IR absorption at 1655 cm^{-1} (d) Lignin and starch distribution based on the IR absorption at 1461 cm^{-1}. The IR adsorption intensity increases from red to blue. Scale bar = 20 μm

This study demonstrates the potential of FTIR microspectroscopy on food by-products with varying levels of cell wall disruption. Based on the relative intensity of the signals, we have identified the macroconstituents of food by-products. The compounds identified as the predominant constituents align with the findings reported in the literature for the three materials examined [7, 11, 16]. Future studies will need

to focus on the quantification of targeted compounds in comparison to established analytical methods. Although the limited resolution of the optical objectives of FTIR microspectrometers due to the diffraction limit [38] hinders the differentiation of some structures, other microscopic techniques, such as BF or CLSM, can be employed to obtain complementary information that helps overcome this limitation. Frozen sectioning proved to be a feasible sample preparation for FTIR microspectroscopy that requires minimal processing. Traditionally, biological samples are preserved using chemicals such as formalin or ethanol to prevent degradation of the cell structure and aid in the preparation of intact sections [30]. However, in this study, untreated frozen food by-products were used. The consistency of the spectral information and the similarity of the micrographs with literature studies support this approach. The use of chemical fixatives can alter the infrared spectrum or mask signals, and their removal can lead to the loss of compounds [25, 30]. The use of frozen sectioning avoids alterations in spectral information, but caution is needed when concluding solely based on microscopic information. Freezing can lead to artifact generation due to the formation of ice crystals that alter the structure of the cell wall [41], and some cells may break during sectioning. Given the limited spatial resolution of FTIR microspectroscopy, this effect may be overlooked; however, it is relevant for complementary imaging techniques. Ice crystal damage might alter autofluorescence signals by disrupting native fluorophores, thereby constraining the utility of autofluorescence based imaging methods. In addition, a poor adhesion of the tissue sections to the support material can hinder the acquisition of robust data. Preliminary tests must be conducted when working with new samples to determine the optimal support material. Despite its limitations, frozen sectioning offers significant advantages as a sample preparation method for FTIR microspectroscopy studies of food by-products. Its ease of implementation, rapid processing time, and absence of chemical fixatives make it an advantageous

approach to exploring the chemical composition and spatial distribution of valuable compounds.

The removal of the signals related to the sample-free areas was considered beneficial as a noise removal method. In this way, a representative average spectrum could be obtained, providing information about the global composition of the sample that can be used to explore the spatial location of selected compounds further.

Our results display the capability of FTIR microspectroscopy to assess the spatial distribution of target compounds with potential industrial applications. Based on our findings, we believe that the use of this protocol for manufacturing is feasible; however, it requires optimization for each new stream. Therefore, it would be advantageous to implement this in facilities that handle only a limited variety of by-products. Sample preparation is specific to each type of sample, demanding optimization for every new biomass due to differences in physical characteristics and cell wall disruption. With advancements in data science and AI, the automation of data acquisition, treatment, and interpretation can be achieved with relative ease [68]. Overall, we believe this method could be applied as a routine analysis to some extent, allowing for the monitoring of variations in biomass. However, it proves to be more robust in developing processes, where optimal extraction parameters must be determined and adjusted. The findings indicate the potential of FTIR microspectroscopy as an effective method for monitoring the composition of food by-products at various stages of the valorization process. This technique provides valuable insights that could facilitate the development of robust valorization processes.

4 Conclusions

Transmission FTIR microspectroscopy was applied to assess the chemical composition of a series of industrial food by-products, in particular potato trimmings, carrot pomace and brewer's spent grain. It allowed the simultaneous investigation of the

major constituents and their spatial distribution with minimal sample preparation. Samples were prepared by frozen sectioning with a small amount of OCT as a support medium to prevent chemical contamination. Following microscopic evaluation, absorption profiles were recorded, and hierarchical cluster analysis was employed to differentiate spectral information related to the sample from the support material. This approach enabled the determination of a representative average spectrum. Comparison of the representative average spectra of sample replicates collected on different days showed good reproducibility of the method as absorbance peaks retained the same wavenumber. The derivative FTIR spectra revealed previously hidden information beneath the broader peaks of the spectra, providing information about functional groups within the samples. However, some macroconstituents provided overlapping signals, making it difficult to assign the absorption signals to individual components. Despite improvements in technology, the light diffraction limit affects the FTIR microspectroscopy capability of resolving intracellular structures in individual cells. For more comprehensive studies, the hypotheses generated by this technique require validation through complementary methods. Advanced technologies such as nano-FTIR effectively address resolution challenges; however, they necessitate prolonged acquisition times, making them less advisable for routine analysis of large sections [69]. Therefore, microscopic techniques such as BF or CLSM are better suited to provide complementary information.

The proposed methodology demonstrates that FTIR microspectroscopy is an effective technique for semi-quantitatively identifying a wide range of compounds with industrial significance. It can be applied to characterize food by-products during various stages of the valorization process, thereby providing valuable information on separation efficiency and stabilization aspects of novel green recovery methods.

Supplementary information. Supplementary information can be found below

Acknowledgements. The authors would like to acknowledge Baptiste Vanleenhove, Ben Van den Wouwer, Elien de Laet and Chenxu Guo for providing the samples utilised in this project. The authors would like to acknowledge Martine Vanhamel for technical support with FTIR analysis.

Declarations

- Funding The authors wish to thank VLAIO and Flanders' FOOD for the funding and support received for this work performed in the framework of the cSBO project *EffSep* (grant number HBC.2019.0012).
- Conflict of interest The authors declare no competing interests.
- Ethics approval and consent to participate Not applicable
- Consent for publication All authors have read and agreed to the published version of the manuscript.
- Author contribution Paula Varas Perez: conceptualization (lead), methodology, investigation, data curation, formal analysis, validation, writing- original draft. Alexis Fagot: investigation, data curation, formal analysis, writing-review and editing. Martijn Heleven: investigation, writing-review and editing. Karen Smeet: investigation, writing-review and editing. Pieter Samyn: writing-review and editing. Peter Adriaensens: writing-review and editing. Wouter Marchal: conceptualization, supervision, writing-review and editing. Dries Vandamme: funding acquisition, conceptualization, resources, supervision, writing-review and editing.
- Data availability Not applicable
- Materials availability Not applicable
- Code availability Not applicable

Appendix A Adhesion Brewer's spent grain

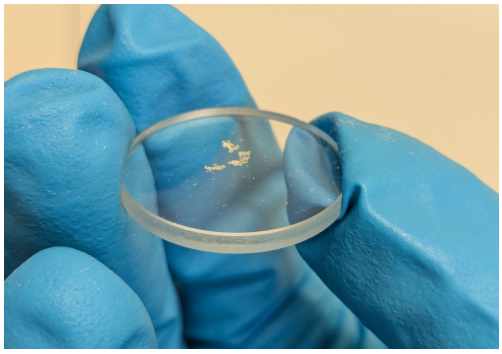

Fig. A1 Brewer's spent grain cryosection transfered to CaF_2 crystal. Poor adherence is observed

Appendix B Brewer's spent grain

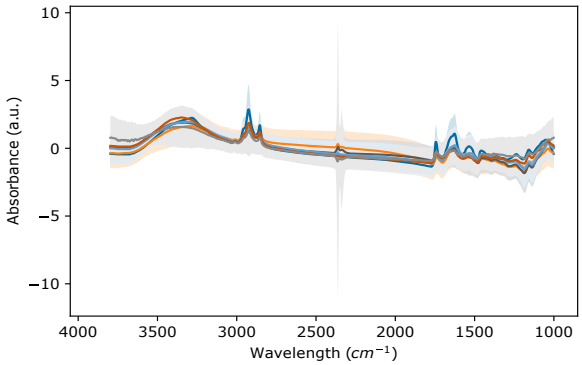

Fig. B2 Representative average spectra with 95% confidence interval obtained for all the BSG samples using hierarchical cluster analysis. The colored area indicates the 95% confidence interval

Appendix C Carrot pomace

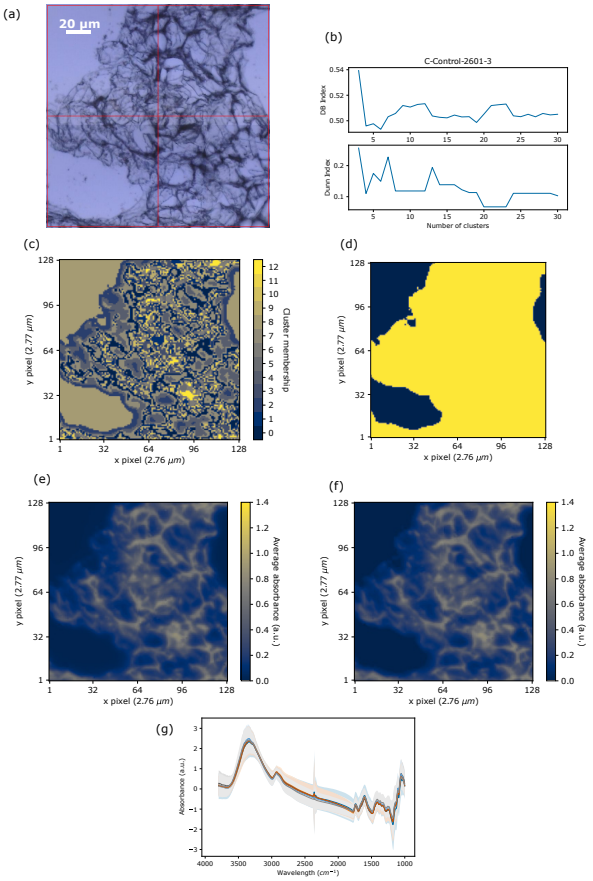

Fig. C3 (a) Example of micrograph of carrot pomace sample where the areas free of sample are visible in light gray. (b) Evolution of the Davies-Bouldin (top) and Dunn (bottom) indexes with the increasing number of clusters for the sample. The minimum of the Davies-Bouldin index is reached for 3 clusters while the maximum of the Dunn index is reached for 6 clusters. Nevertheless, 13 clusters were chosen as it is a local maximum of the Dunn index while the Davies-Bouldin stays low. This number of clusters allows to avoid excessive filtering in the low intensity region. (c) Clustering performed on the sample where pixels in the cluster 8 correspond to the areas without sample. (d) Corresponding mask used for the filtering with areas in black to be filtered out and areas in yellow corresponding to the sample (e) Average absorbance intensity map of the sample. (f) Resulting average absorbance heatmap after filtering. In both (e) and (f), the scale goes from low intensity in black to high intensity in yellow. (g) Representative average spectra with 95% confidence interval obtained for all the carrot pomace samples using hierarchical cluster analysis. The colored area indicates the 95% confidence interval.

Appendix D Potato trimming

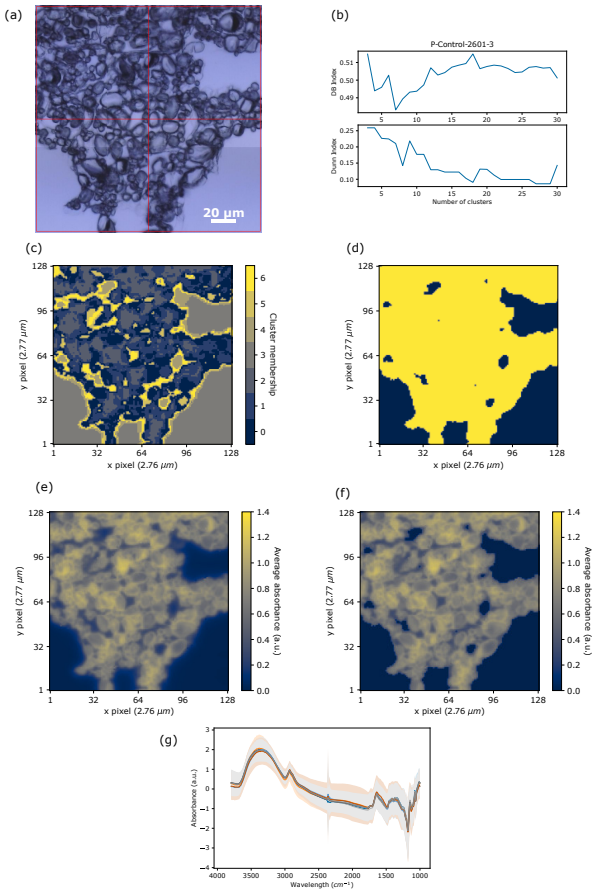

Fig. D4 (a) Example of a micrograph of potato trimmings sample where the areas free of sample are visible in light gray. (b) Evolution of the Davies-Bouldin (top) and Dunn (bottom) indexes with the increasing number of clusters for the sample. The minimum of the Davies-Bouldin index is reached for 7 clusters while the maximum of the Dunn index is reached for 3 oand 4 clusters. The best results were achieved with 7 clusters. (c) Clustering performed on the potato trimming sample of where pixels in the clusters 3 and 4 correspond to the areas without sample. (d) Corresponding mask used for the filtering with areas in black to be filtered out and areas in yellow corresponding to the sample. (e) Average absorbance intensity map of the sample. (f) Resulting average absorbance heatmap after filtering. In both (e) and (f), the scale goes from low intensity in black to high intensity in yellow. (g) Representative average spectra with 95% confidence interval obtained for all the PT samples using hierarchical cluster analysis. The colored area indicates the 95% confidence interval.

Appendix E Reproducibility

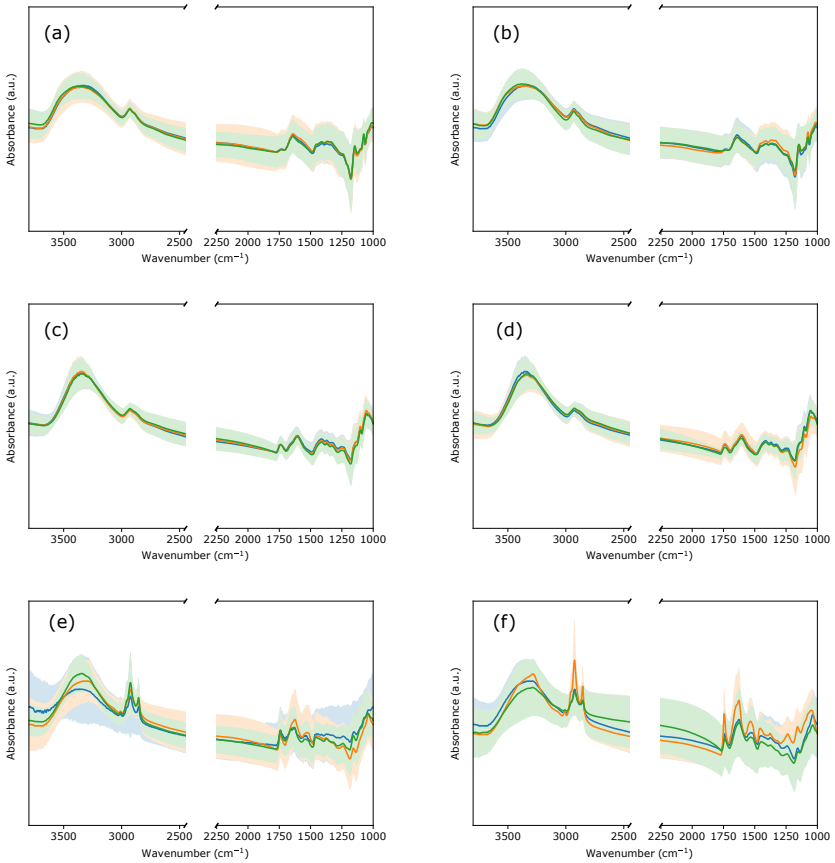

Fig. E5 Average FTIR spectra and the 95% confidence interval calculated of three technical replicates obtained on the same day (a,c, and e) and on different days (b,d, and f) for potato trimmings (PT) (a,b), carrot pomace (CP) (c,d) and brewer's spent grain (BSG) (e,f). The colored areas indicate the 95% confidence interval. The spectra were offset and the region between 2500-2250 cm^{-1}, where CO_2 signals are located, was removed for clarification

	Mean	Standard Deviation	Mean	Standard Deviation	Mean	Standard Deviation
	1746 cm-1		1461 cm-1		1235 cm-1	
Potato Trimmings	- 0.90	0.33	- 0.63	0.41	- 0.98	0.50
	- 0.88	0.32	-0.67	0.41	- 1.13	0.47
	1746 cm-1		1369 cm-1		1158 cm-1	
Carrot Pomace	-0.75	0.30	-0.73	0.25	-1.26	0.60
	-0.87	0.19	-0.73	0.20	-1.03	0.44
	1746 cm-1		1461 cm-1			
Brewer's Spent Grain	-0.71	0.65	-0.84	0.56		
	-0.33	0.55	-0.44	0.57		

Table E1 Examples of the mean value and standard deviation of selected signal intensities for otato trimmings (PT), carrot pomace (CP)and brewer's spent grain (BSG)

Appendix F Average infrared spectra of food by-products

The representative average spectra of CP, PT, and BSG are shown in Fig. F6.

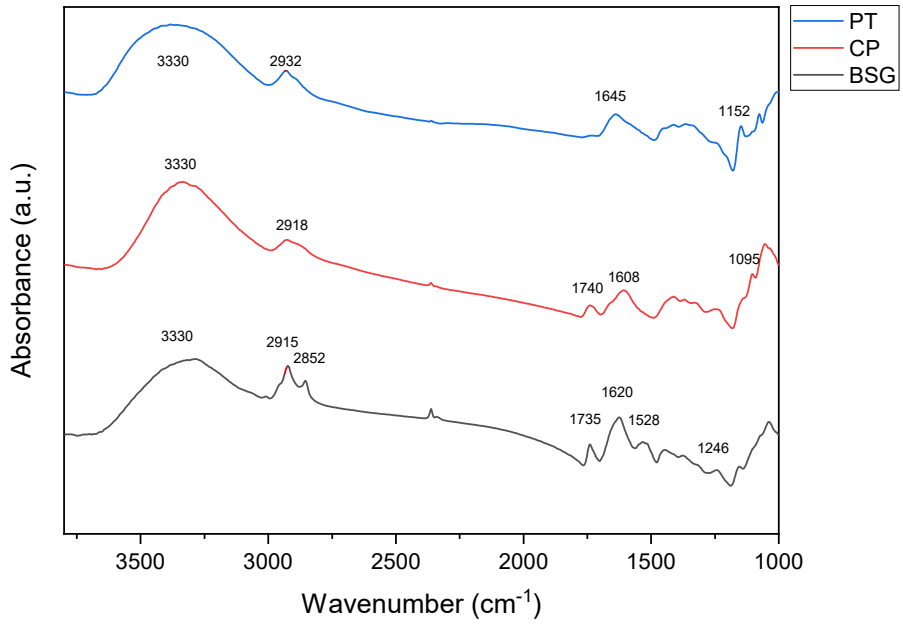

Fig. F6 Average infrared spectra of potato trimmings (PT), carrot pomace (CP) and brewer's spent grain (BSG) represented in blue, red and black, respectively. The spectra were offset for clarification

The chemical specificity of FTIR microspectroscopy enables the identification of the major constituents of food by-products by correlating the observed signals with relevant components found in the literature, which are summarized in Table F2.

Table F2 List of the relevant components and their observed signals as found in the literature

Wavenumber (cm^{-1})	Vibrational Mode	Characteristic Compounds	References
3600-3300	O-H, N-H stretching	Polysaccharides, water, phenolic compounds, proteins	[4,8]
3000-2800	CH_2 and CH_3 stretching	Lipids, proteins, polysaccharides	[5]
1740-1705	C=O stretching	Lipids, pectin	[1,2]
1650	C=O stretching	Amide I (protein)	[7]
1528	N-H bending, C-N stretching	Amide II (protein)	[6,7]
1470	CH_2 deformation	Lipids	[1]
1246	N-H bending, C-N stretching	Amide III (protein)	[3,7]
1170	C-O, C-C, C-OH stretching	Lipids	[1]
1150	C-O, C-C, C-OH stretching	Starch, cellulose, hemicellulose, pectin	[4]
1100-1000	C-O-H bending	Starch, cellulose, hemicellulose, pectin	[4,11]

Appendix G Chemical imaging BSG

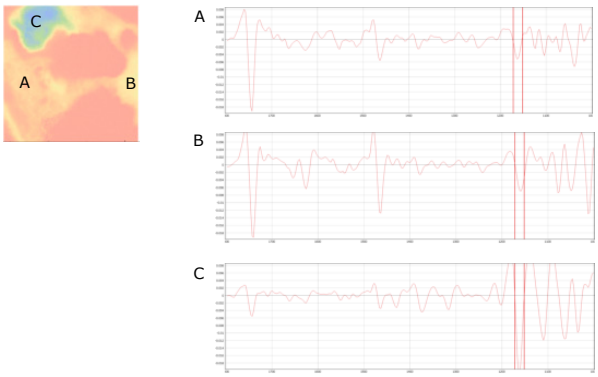

Fig. G7 Chemical visualization of the peak 1160 cm^{-1} and second derivative spectra of selected pixels in different parts of the sample. The intensity of the peak 1463 cm^{-1} in the second derivative spectra C is lower compared with the intensity of the peak 1160 cm^{-1} and low intensity is found in the peak 1763 cm-1, which is characteristic of starch [9]

Appendix H Chemical imaging BSG-peak 1510 cm^{-1}

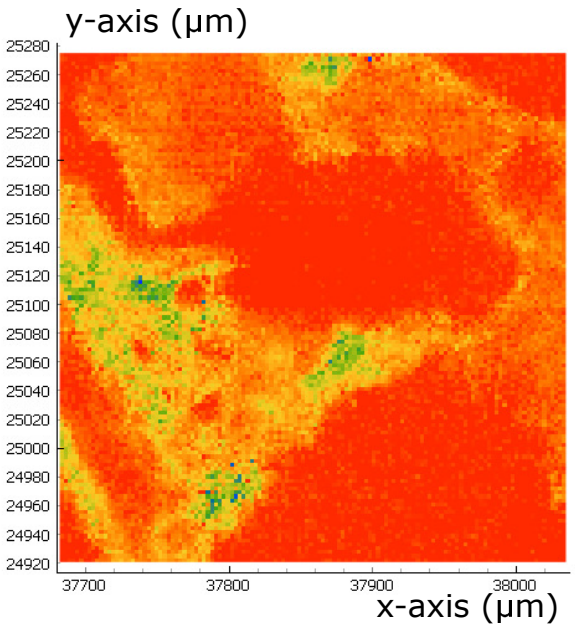

Fig. H8 False color map associated with the peak 1510 cm^{-1}. This signal corresponds to the aromatic skeletal vibration of lignin and phenolic compounds. Smaller high intensity regions can be observed in the endosperm in concordance with Yu et al. (2004) [10]

Appendix I References

[1] Bağcıoğlu, M., Kohler, A., Seifert, S., Kneipp, J., Zimmermann, B.: Monitoring of plant–environment interactions by high-throughput FTIR spectroscopy of pollen. *Methods in Ecology and Evolution* **8**(7), 870–880 (2017). https://doi.org/10.1111/2041-210X.12697

[2] Beć, K.B., Grabska, J., Bonn, G.K., Popp, M., Huck, C.W.: Principles and applications of vibrational spectroscopic imaging in plant science: A review. *Frontiers in Plant Science* **11** (2020). https://doi.org/10.3389/fpls.2020.01226

[3] Cai, S., Singh, B.R.: A distinct utility of the amide III infrared band for secondary structure estimation of aqueous protein solutions using partial least squares methods. *Biochemistry* **43**(9), 2541–2549 (2004). https://doi.org/10.1021/bi030149y

[4] Canteri, M.H.G., Renard, C.M.G.C., Le Bourvellec, C., Bureau, S.: ATR-FTIR spectroscopy to determine cell wall composition: Application on a large diversity of fruits and vegetables. *Carbohydrate Polymers* **212**, 186–196 (2019). https://doi.org/10.1016/j.carbpol.2019.02.021

[5] Gorgulu, S.T., Dogan, M., Severcan, F.: The characterization and differentiation of higher plants by Fourier transform infrared spectroscopy. *Applied Spectroscopy* **61**(3), 300–308 (2007). https://doi.org/10.1366/000370207780220903

[6] Ji, Y., Yang, X., Ji, Z., Zhu, L., Ma, N., Chen, D., Jia, X., Tang, J., Cao, Y.: DFT-calculated IR spectrum amide I, II, and III band contributions of N-methylacetamide fine components. *ACS Omega* **5**(15), 8572–8578 (2020). https://doi.org/10.1021/acsomega.9b04421

[7] Mallamace, F., Corsaro, C., Mallamace, D., Vasi, S., Vasi, C., Dugo, G.: The role of water in protein's behavior: The two dynamical crossovers studied by NMR and FTIR techniques. *Computational and Structural Biotechnology Journal* **13**, 33–37 (2015). https://doi.org/10.1016/j.csbj.2014.11.007

[8] Szymanska-Chargot, M., Zdunek, A.: Use of FT-IR spectra and PCA for the bulk characterization of cell wall residues of fruits and vegetables along a fraction process. *Food Biophysics* **8**(1), 29–42 (2013). https://doi.org/10.1007/s11483-012-9279-7

[9] Warren, F.J., Gidley, M.J., Flanagan, B.M.: Infrared spectroscopy as a tool to characterise starch ordered structure—a joint FTIR–ATR, NMR, XRD and DSC study. *Carbohydrate Polymers* **139**, 35–42 (2016). https://doi.org/10.1016/j.carbpol.2015.11.066

[10] Yu, P., McKinnon, J.J., Christensen, C.R., Christensen, D.A.: Using Synchrotron Transmission FTIR Microspectroscopy as a rapid, direct, and nondestructive

analytical technique to reveal molecular microstructural-chemical features within tissue in grain barley. *Journal of Agricultural and Food Chemistry* **52**(6), 1484–1494 (2004). https://doi.org/10.1021/jf035065a

[11] Zhu, J., Wang, H., Guo, F., Salmén, L., Yu, Y.: Cell wall polymer distribution in bamboo visualized with *in situ* imaging FTIR. *Carbohydrate Polymers* **274**, 118653 (2021). https://doi.org/10.1016/j.carbpol.2021.118653

References

[1] Eurostat: Food waste and food waste prevention - estimates (2023). https://ec.europa.eu/eurostat/statistics-explained/index.php?title=Food_waste_and_food_waste_prevention_-_estimates#Amounts_of_food_waste_at_EU_level Accessed 27-06-2024

[2] Dinani, S.T., Goot, A.J.: Challenges and solutions of extracting value-added ingredients from fruit and vegetable by-products: a review. Critical Reviews in Food Science and Nutrition **63**(25), 7749–7771 (2023) https://doi.org/10.1080/10408398.2022.2049692

[3] Sadh, P.K., Duhan, S., Duhan, J.S.: Agro-industrial wastes and their utilization using solid state fermentation: a review. Bioresources and Bioprocessing **5**(1), 1 (2018) https://doi.org/10.1186/s40643-017-0187-z

[4] Patel, A., Mikes, F., Bühler, S., Matsakas, L.: Valorization of brewers' spent grain for the production of lipids by oleaginous yeast. Molecules **23**(12) (2018) https://doi.org/10.3390/molecules23123052

[5] Rayón, E., Ferrandiz, S., Rico, M.I., López, J., P. Arrieta, M.: Microstructure, mechanical, and thermogravimetric characterization of cellulosic by-products obtained from biomass seeds. International Journal of Food Properties **18**(6), 1211–1222 (2015) https://doi.org/10.1080/10942912.2014.884578 https://doi.org/10.1080/10942912.2014.884578

[6] Faeghe, J., Faramarz, K., Hossein, K., Seyed, S.H.: Pectin from carrot pomace: Optimization of extraction and physicochemical properties. Carbohydrate Polymers **157**, 1315–1322 (2017) https://doi.org/10.1016/j.carbpol.2016.11.013

[7] Parchami, M., Ferreira, J.A., Taherzadeh, M.J.: Starch and protein recovery from brewer's spent grain using hydrothermal pretreatment and their conversion to edible filamentous fungi – a brewery biorefinery concept. Bioresource Technology **337**, 125409 (2021) https://doi.org/10.1016/j.biortech.2021.125409

[8] Bond, J., Putnam, P.A.: Nutritive value of dehydrated sweet potato trimmings fed to beef steers. Journal of Agricultural and Food Chemistry **15**(4), 726–728 (1967) https://doi.org/10.1021/jf60152a002 https://doi.org/10.1021/jf60152a002

[9] Janssens, S.R.M., Smit, A.B.: Reststromen Consumptieaardappelen. Factsheet / LEI Wageningen UR : 2016-013a. LEI, 905, LEI Consument & Keten, (2016). https://edepot.wur.nl/368097

[10] Food and Agriculture Organization of the United Nations: FAOSTAT: Crops and Livestock Products. Accessed: 2024-10-08 (2024). https://www.fao.org/faostat/en/#data/QCL

[11] Leonel, M., Carmo, E.L., Fernandes, A.M., Soratto, R.P., Ebúrneo, J.A.M., Garcia, É.L., Santos, T.P.R.: Chemical composition of potato tubers: the effect of cultivars and growth conditions. Journal of Food Science and Technology **54**(8),

2372–2378 (2017) https://doi.org/10.1007/s13197-017-2677-6

[12] Amoroso, L., De France, K.J., Milz, C.I., Siqueira, G., Zimmermann, T., Nyström, G.: Sustainable Cellulose Nanofiber Films from Carrot Pomace as Sprayable Coatings for Food Packaging Applications. ACS Sustainable Chemistry & Engineering **10**(1), 342–352 (2022) https://doi.org/10.1021/acssuschemeng.1c06345

[13] Kosters, P.S.R., Waldron, K.W.: 15 - production of high-value functional vegetable juices from food co-products. In: Waldron, K. (ed.) Handbook of Waste Management and Co-Product Recovery in Food Processing. Woodhead Publishing Series in Food Science, Technology and Nutrition, pp. 376–390. Woodhead Publishing, Sawston (2009). https://doi.org/10.1533/9781845697051.3.376

[14] Priyadarshini, A., Priyadarshini, A.: Chapter 2 - market dimensions of the fruit juice industry. In: Rajauria, G., Tiwari, B.K. (eds.) Fruit Juices, pp. 15–32. Academic Press, San Diego (2018). https://doi.org/10.1016/B978-0-12-802230-6.00002-3

[15] Di Giacomo, G., Taglieri, L.: A New High-Yield Process for the Industrial Production of Carrot Juice. Food and Bioprocess Technology **2**(4), 441–446 (2009) https://doi.org/10.1007/s11947-009-0207-x

[16] Luca, M.I., Ungureanu-Iuga, M., Mironeasa, S.: Carrot pomace characterization for application in cereal-based products. Applied Sciences **12**(16) (2022) https://doi.org/10.3390/app12167989

[17] Verni, M., Pontonio, E., Krona, A., Jacob, S., Pinto, D., Rinaldi, F., Verardo, V., Díaz-de-Cerio, E., Coda, R., Rizzello, C.G.: Bioprocessing of brewers' spent grain enhances its antioxidant activity: Characterization of phenolic compounds and bioactive peptides. Frontiers in Microbiology **11** (2020) https://doi.org/10.

3389/fmicb.2020.01831

[18] Silbir, S., Goksungur, Y.: Natural red pigment production by monascus purpureus in submerged fermentation systems using a food industry waste: Brewer's spent grain. Foods **8**(5) (2019) https://doi.org/10.3390/foods8050161

[19] Ikram, A., Rasheed, A., Khan, A.A., Khan, R., Ahmad, M., Bashir, R., Mohamed, M.H.: Exploring the health benefits and utility of carrots and carrot pomace: a systematic review. International Journal of Food Properties **27**(1), 180–193 (2024) https://doi.org/10.1080/10942912.2023.2301569

[20] Vanleenhove, B., Van den Wouwer, B., Verwee, E., Slachmuylders, L., Joossens, M., Brijs, K., Dewettinck, K., De Meester, S., Raes, K.: Impact of potato trimming acidification on protein characteristics and bacterial community during long-term storage. LWT **191**, 115572 (2024) https://doi.org/10.1016/j.lwt.2023.115572

[21] De Laet, E., Bernaerts, T., Dewettinck, K., Hendrickx, M.E., Van Loey, A.M.: The effect of different particle size reduction techniques on the biomass microstructure and the influence on the pectin extraction yield and structure. Food Hydrocolloids **151**, 109875 (2024) https://doi.org/10.1016/j.foodhyd.2024.109875

[22] Reche, C., Rosselló, C., Dalmau, E., Eim, V., Simal, S.: Quantification of microstructural changes in artichoke by-products by image analysis after high-power ultrasound-assisted extraction of bioactive compounds. LWT **171**, 114127 (2022) https://doi.org/10.1016/j.lwt.2022.114127

[23] Verwee, E., Vanleenhove, B., Van den Wouwer, B., Van de Walle, D., Brijs, K., Raes, K., Damme, E.J.M.V., Dewettinck, K., Skirtach, A.G.: Microscopic study of proteins, starch and cell walls in potato trimmings. LWT **209**, 116798 (2024) https://doi.org/10.1016/j.lwt.2024.116798

[24] Belardi, I., Marrocchi, A., Alfeo, V., Sileoni, V., De Francesco, G., Paolantoni, M., Marconi, O.: Sequential extraction and attenuated total reflection–fourier transform infrared spectroscopy monitoring in the biorefining of brewer's spent grain. Molecules **28**(24) (2023) https://doi.org/10.3390/molecules28247992

[25] Baker, M.J., Trevisan, J., Bassan, P., Bhargava, R., Butler, H.J., Dorling, K.M., Fielden, P.R., Fogarty, S.W., Fullwood, N.J., Heys, K.A., Hughes, C., Lasch, P., Martin-Hirsch, P.L., Obinaju, B., Sockalingum, G.D., Sulé-Suso, J., Strong, R.J., Walsh, M.J., Wood, B.R., Gardner, P., Martin, F.L.: Using Fourier transform IR spectroscopy to analyze biological materials. Nature Protocols **9**(8), 1771–1791 (2014) https://doi.org/10.1038/nprot.2014.110

[26] Siregar, S., Nurhikmat, A., Amdani, R.Z., Hatmi, R.U., Kobarsih, M., Kusumaningrum, A., Karim, M.A., Dameswari, A.H., Siswanto, N., Siswoprayogi, S., Yuliyanto, P.: Estimation of proximate composition in rice using atr-ftir spectroscopy and chemometrics. ACS Omega **9**(30), 32760–32768 (2024) https://doi.org/10.1021/acsomega.4c02816

[27] Yu, P., McKinnon, J.J., Christensen, C.R., Christensen, D.A.: Using synchrotron transmission ftir microspectroscopy as a rapid, direct, and nondestructive analytical technique to reveal molecular microstructural-chemical features within tissue in grain barley. Journal of Agricultural and Food Chemistry **52**(6), 1484–1494 (2004) https://doi.org/10.1021/jf035065a

[28] Zhu, J., Wang, H., Guo, F., Salmén, L., Yu, Y.: Cell wall polymer distribution in bamboo visualized with in situ imaging ftir. Carbohydrate Polymers **274**, 118653 (2021) https://doi.org/10.1016/j.carbpol.2021.118653

[29] Wang, F., Wang, C., Song, S.: A study of starch content detection and the visualization of fresh-cut potato based on hyperspectral imaging. RSC Adv. **11**,

13636–13643 (2021) https://doi.org/10.1039/D1RA01013A

[30] Zohdi, V., Whelan, D.R., Wood, B.R., Pearson, J.T., Bambery, K.R., Black, M.J.: Importance of tissue preparation methods in ftir micro-spectroscopical analysis of biological tissues: 'traps for new users'. PLOS ONE **10**(2), 1–11 (2015) https://doi.org/10.1371/journal.pone.0116491

[31] Liyanage, S., Dassanayake, R.S., Bouyanfif, A., Rajakaruna, E., Ramalingam, L., Moustaid-Moussa, N., Abidi, N.: Optimization and validation of cryostat temperature conditions for trans-reflectance mode ftir microspectroscopic imaging of biological tissues. MethodsX **4**, 118–127 (2017) https://doi.org/10.1016/j.mex.2017.01.006

[32] Kohler, A., Bertrand, D., Martens, H., Hannesson, K., Kirschner, C., Ofstad, R.: Multivariate image analysis of a set of FTIR microspectroscopy images of aged bovine muscle tissue combining image and design information. Analytical and Bioanalytical Chemistry **389**(4), 1143–1153 (2007) https://doi.org/10.1007/s00216-007-1414-9

[33] Toplak, M., Read, S.T., Sandt, C., Borondics, F.: Quasar: Easy machine learning for biospectroscopy. Cells **10**(9) (2021) https://doi.org/10.3390/cells10092300

[34] Banas, K., Banas, A., Gajda, M., Pawlicki, B., Kwiatek, W.M., Breese, M.B.H.: Pre-processing of fourier transform infrared spectra by means of multivariate analysis implemented in the r environment. Analyst **140**, 2810–2814 (2015) https://doi.org/10.1039/C5AN00002E

[35] Foundation, P.S.: Python: a high-level, general-purpose programming language. (2008). https://www.python.org/

[36] Team, S.D.: Spyder: The Scientific Python Development Environment. Version

5.x (2023). https://www.spyder-ide.org/

[37] Demšar, J., Curk, T., Erjavec, A., Gorup, Hočevar, T., Milutinovič, M., Možina, M., Polajnar, M., Toplak, M., Starič, A., Štajdohar, M., Umek, L., Žagar, L., Žbontar, J., Žitnik, M., Zupan, B.: Orange: Data mining toolbox in python. Journal of Machine Learning Research **14**, 2349–2353 (2013)

[38] Lasch, P., Naumann, D.: Spatial resolution in infrared microspectroscopic imaging of tissues. Biochimica et Biophysica Acta (BBA) - Biomembranes **1758**(7), 814–829 (2006) https://doi.org/10.1016/j.bbamem.2006.06.008 . Vibrational Microscopic Imaging: Towards Molecular Pathology

[39] Sjöö, Malin and Eliasson, Ann-Charlotte and Autio, Karin: Comparison of different microscopic methods for the study of starch and other components within potato cells. Food **3**(special issue 1), 39–44 (2009)

[40] Bordoloi, A., Kaur, L., Singh, J.: Parenchyma cell microstructure and textural characteristics of raw and cooked potatoes. Food Chemistry **133**(4), 1092–1100 (2012) https://doi.org/10.1016/j.foodchem.2011.11.044 . Advances in Potato Chemistry, Nutrition and Technology

[41] Préstamo, G., Fuster, C., Risueño, M.C.: Effects of blanching and freezing on the structure of carrots cells and their implications for food processing. Journal of the Science of Food and Agriculture **77**(2), 223–229 (1998) https://doi.org/10.1002/(SICI)1097-0010(199806)77:2⟨223::AID-JSFA29⟩3.0.CO;2-2

[42] Sucheta, Misra, N.N., Yadav, S.K.: Extraction of pectin from black carrot pomace using intermittent microwave, ultrasound and conventional heating: Kinetics, characterization and process economics. Food Hydrocolloids **102**, 105592 (2020) https://doi.org/10.1016/j.foodhyd.2019.105592

[43] Sun, Y., Kang, X., Chen, F., Liao, X., Hu, X.: Mechanisms of carrot texture alteration induced by pure effect of high pressure processing. Innovative Food Science & Emerging Technologies **54**, 260–269 (2019) https://doi.org/10.1016/j.ifset.2018.08.012

[44] Knockaert, G., Lemmens, L., Van Buggenhout, S., Hendrickx, M., Van Loey, A.: Changes in β-carotene bioaccessibility and concentration during processing of carrot puree. Food Chemistry **133**(1), 60–67 (2012) https://doi.org/10.1016/j.foodchem.2011.12.066

[45] Forssell, P., Kontkanen, H., Schols, H.A., Hinz, S., Eijsink, V.G.H., Treimo, J., Robertson, J.A., Waldron, K.W., Faulds, C.B., Buchert, J.: Hydrolysis of brewers' spent grain by carbohydrate degrading enzymes. Journal of the Institute of Brewing **114**(4), 306–314 (2008) https://doi.org/10.1002/j.2050-0416.2008.tb00774.x

[46] Ribeiro-Sanches, M.A., Stochi, V.A.L., Borges-Machado, A.L., Augusto, P.E.D., Polachini, T.C., Telis-Romero, J.: Valorization of brewer's spent grains (bsg) through alkaline hydrogen peroxide processing: Effect on composition, structure and rheological properties. Food and Bioproducts Processing **147**, 239–250 (2024) https://doi.org/10.1016/j.fbp.2024.07.008

[47] Jääskeläinen, A.-S., Holopainen-Mantila, U., Tamminen, T., Vuorinen, T.: Endosperm and aleurone cell structure in barley and wheat as studied by optical and raman microscopy. Journal of Cereal Science **57**(3), 543–550 (2013) https://doi.org/10.1016/j.jcs.2013.02.007

[48] Ratajczak, K., Juzwa, W., Piotrowska-Cyplik, A.: Optimization of the flow cytometry method of detection, quantification and qualification of microorganisms in carrot juice. Food Chemistry **460**, 140606 (2024) https://doi.org/10.1016/

j.foodchem.2024.140606

[49] Xie, P., Yang, Y., Oyom, W., Su, T., Tang, Y., Wang, Y., Li, Y., Prusky, D., Bi, Y.: Chitooligosaccharide accelerated wound healing in potato tubers by promoting the deposition of suberin polyphenols and lignin at wounds. Plant Physiology and Biochemistry **199**, 107714 (2023) https://doi.org/10.1016/j.plaphy.2023.107714

[50] Donaldson, L.: Autofluorescence in plants. Molecules **25**(10) (2020) https://doi.org/10.3390/molecules25102393

[51] Dunn, J.C.: A fuzzy relative of the isodata process and its use in detecting compact well-separated clusters. Journal of Cybernetics **3**(3), 32–57 (1973) https://doi.org/10.1080/01969727308546046

[52] Olivieri, A.C., Escandar, G.M.: Chapter 6 - analytical figures of merit. In: Olivieri, A.C., Escandar, G.M. (eds.) Practical Three-Way Calibration, pp. 93–107. Elsevier, Boston (2014). https://doi.org/10.1016/B978-0-12-410408-2.00006-5

[53] Davies, D.L., Bouldin, D.W.: A cluster separation measure. IEEE Transactions on Pattern Analysis and Machine Intelligence **PAMI-1**(2), 224–227 (1979) https://doi.org/10.1109/TPAMI.1979.4766909

[54] Liang, S., McDonald, A.G.: Chemical and thermal characterization of potato peel waste and its fermentation residue as potential resources for biofuel and bioproducts production. Journal of Agricultural and Food Chemistry **62**(33), 8421–8429 (2014) https://doi.org/10.1021/jf5019406

[55] Szymanska-Chargot, M., Zdunek, A.: Use of FT-IR Spectra and PCA to the Bulk Characterization of Cell Wall Residues of Fruits and Vegetables Along a Fraction Process. Food biophysics **8**(1), 29–42 (2013) https://doi.org/10.1007/s11483-012-9279-7

[56] Canteri, M.H.G., Renard, C.M.G.C., Le Bourvellec, C., Bureau, S.: Atr-ftir spectroscopy to determine cell wall composition: Application on a large diversity of fruits and vegetables. Carbohydrate Polymers **212**, 186–196 (2019) https://doi.org/10.1016/j.carbpol.2019.02.021

[57] Beć, K.B., Grabska, J., Bonn, G.K., Popp, M., Huck, C.W.: Principles and applications of vibrational spectroscopic imaging in plant science: A review. Frontiers in Plant Science **11** (2020) https://doi.org/10.3389/fpls.2020.01226

[58] Kizil, R., Irudayaraj, J., Seetharaman, K.: Characterization of irradiated starches by using ft-raman and ftir spectroscopy. Journal of Agricultural and Food Chemistry **50**(14), 3912–3918 (2002) https://doi.org/10.1021/jf011652p

[59] Quijano-Ortega, N., Fuenmayor, C.A., Zuluaga-Dominguez, C., Diaz-Moreno, C., Ortiz-Grisales, S., García-Mahecha, M., Grassi, S.: Ftir-atr spectroscopy combined with multivariate regression modeling as a preliminary approach for carotenoids determination in cucurbita spp. Applied Sciences **10**(11) (2020) https://doi.org/10.3390/app10113722

[60] Cybulska, J., Zdunek, A., Kozioł, A.: The self-assembled network and physiological degradation of pectins in carrot cell walls. Food Hydrocolloids **43**, 41–50 (2015) https://doi.org/10.1016/j.foodhyd.2014.04.032

[61] Outeiriño, D., Costa-Trigo, I., Rodríguez, A., Pérez Guerra, N., Domínguez, J.M.: Recovery and reuse of ionic liquid cholinium glycinate in the treatment of brewery spent grain. Separation and Purification Technology **254**, 117651 (2021) https://doi.org/10.1016/j.seppur.2020.117651

[62] Lal, M.K., Kumar, A., Jena, R., Dutt, S., Thakur, N., Parmar, V., Kumar, V., Singh, B.: Lipids in potato. In: Raigond, P., Singh, B., Dutt, S., Chakrabarti,

S.K. (eds.) Potato: Nutrition and Food Security, pp. 73–85. Springer, Singapore (2020). https://doi.org/10.1007/978-981-15-7662-1_5

[63] Järvinen, R., Silvestre, A.J.D., Holopainen, U., Kaimainen, M., Nyyssölä, A., Gil, A.M., Pascoal Neto, C., Lehtinen, P., Buchert, J., Kallio, H.: Suberin of potato (solanum tuberosum var. nikola): Comparison of the effect of cutinase cccut1 with chemical depolymerization. Journal of Agricultural and Food Chemistry **57**(19), 9016–9027 (2009) https://doi.org/10.1021/jf9008907

[64] Christiaens, S., Uwibambe, D., Uyttebroek, M., Van Droogenbroeck, B., Van Loey, A.M., Hendrickx, M.E.: Pectin characterisation in vegetable waste streams: A starting point for waste valorisation in the food industry. LWT - Food Science and Technology **61**(2), 275–282 (2015) https://doi.org/10.1016/j.lwt.2014.12.054

[65] Sadat, A., Joye, I.J.: Peak fitting applied to fourier transform infrared and raman spectroscopic analysis of proteins. Applied Sciences **10**(17) (2020) https://doi.org/10.3390/app10175918

[66] Waglay, A., Karboune, S.: Chapter 4 - potato proteins: Functional food ingredients. In: Singh, J., Kaur, L. (eds.) Advances in Potato Chemistry and Technology (Second Edition), Second edition edn., pp. 75–104. Academic Press, San Diego (2016). https://doi.org/10.1016/B978-0-12-800002-1.00004-2

[67] Jay, A.J., Parker, M.L., Faulks, R., Husband, F., Wilde, P., Smith, A.C., Faulds, C.B., Waldron, K.W.: A systematic micro-dissection of brewers' spent grain. Journal of Cereal Science **47**(2), 357–364 (2008) https://doi.org/10.1016/j.jcs.2007.05.006

[68] Li, H., Xu, S., Teng, J., Jiang, X., Zhang, H., Qin, Y., He, Y., Fan, L.: Deep

learning assisted atr-ftir and raman spectroscopy fusion technology for microplastic identification. Microchemical Journal **212**, 113224 (2025) https://doi.org/10.1016/j.microc.2025.113224

[69] Kästner, B., Schmähling, F., Hornemann, A., Ulrich, G., Hoehl, A., Kruskopf, M., Pierz, K., Raschke, M.B., Wübbeler, G., Elster, C.: Compressed sensing ftir nano-spectroscopy and nano-imaging. Opt. Express **26**(14), 18115–18124 (2018) https://doi.org/10.1364/OE.26.018115